A novel lyotropic liquid crystal formed by triphilic star-polyphiles: hydrophilic/oleophilic/fluorophilic rods arranged in a 12.6.4. tiling†‡

Liliana de Campo,[a] Trond Varslot,[a] Minoo J. Moghaddam,[b] Jacob J. K. Kirkensgaard,[c] Kell Mortensen[c] and Stephen T. Hyde*[a]

Triphilic star-polyphiles are short-chain oligomeric molecules with a radial arrangement of hydrophilic, hydrocarbon and fluorocarbon chains linked to a common centre. They form a number of liquid crystalline structures when mixed with water. In this contribution we focus on a hexagonal liquid crystalline mesophase found in star-polyphiles as compared to the corresponding double-chain surfactant to determine whether the hydrocarbon and fluorocarbon chains are in fact demixed in these star-polyphile systems, or whether both hydrocarbon and fluorocarbon chains are miscible, leading to a single hydrophobic domain, making the star-polyphile effectively amphiphilic. We report SANS contrast variation data that are compatible only with the presence of three distinct immiscible domains within this hexagonal mesophase, confirming that these star-polyphile liquid crystals are indeed hydrophilic/oleophilic/fluorophilic 3-phase systems. Quantitative comparison with scattering simulations shows that the experimental data are in very good agreement with an underlying 2D columnar (12.6.4) tiling. As in a conventional amphiphilic hexagonal mesophase, the hexagonally packed water channels (dodecagonal prismatic domains) are embedded in a hydrophobic matrix, but that matrix is split into oleophilic hexagonal prismatic domains and fluorophilic quadrangular prismatic domains.

Introduction

Liquid crystal self-assembly is mainly driven by the segregation of molecular incompatible subunits into distinct nanodomains. For surfactants forming lyotropic liquid crystals, this incompatibility stems from their amphiphilic character, as they usually contain a hydrophilic and hydrophobic species, and the resulting assemblies are characterised by surfaces separating the two distinct species.[1] Introducing a third incompatible unit into the same molecule, such as a sufficiently long fluorophilic chain, results in polyphilic molecules, offering the potential for a wealth of novel, more complex nanostructured materials. If the immiscible chains are arranged in a star-shaped geometry, the molecular centres which link the multiple radiating chains, must self-assemble along 1D lines, giving rise to 3-phase lines within these self-assemblies in addition to (the usual) two-phase surfaces. For

this reason, we are tempted to call star-polyphilic molecules *linactants* after a suggestion by Richard Templer, analogous to (but distinct from) surfactants. However, this term is already in use for surfactant analogues in two dimensions.[2]

Our prime interest is to generate novel supra-molecular self-assemblies with more than two chemically distinct mesoscale domain types. We have elected to look first at star-polyphiles containing three potentially immiscible chains: fluorocarbon, hydrocarbon and a hydrophilic head-group. A number of hybrid hydrocarbon/fluorocarbon surfactants have been synthesised by other groups[3–8] and many of their solution properties have been investigated.[4,7] These materials have interesting physicochemical properties and applications.[5,7,9] While it is clear that the hydrophilic and hydrophobic moieties in these molecules form spatially segregated domains, the demixing of the hydrophobic domain into an oleophilic and fluorophilic part remains in question, as the surface tension between the oleophilic and fluorophilic domains is much lower than between each of the latter with the hydrophilic domain.[6] Quantifying the demixing of H-domains and F-domains in supramolecular aggregates formed by such small molecules is far from trivial, and some of the results from solution studies of micelles involving mixed hydrocarbon surfactants and fluorocarbon surfactants are still under debate.[10]

In the field of thermotropic liquid crystals, branched bola-amphiphilic T-type and X-type molecules have also elicited a lot of interest.[11] These molecules too can be regarded as polyphilic, because their central aromatic rigid rod constitutes a separate phase, in addition to the hydrophilic and hydrophobic moieties. Of particular relevance to our work reported here is the recent report of an X-shaped Janus-type

[a] Applied Mathematics, Research School of Physical Sciences, Australian National University, Canberra, Australia. E-mail: stephen.hyde@anu.edu.au, liliana.decampo@anu.edu.au
[b] CSIRO Molecular Health Technologies, North Ryde, NSW, Australia
[c] Dept. of Basic Sciences and Environment, Faculty of Life Sciences, Copenhagen University, Copenhagen, Denmark

† This article was submitted as part of a special collection on scattering methods applied to soft matter, marking the 65th birthday of Professor Otto Glatter.
‡ Electronic supplementary information (ESI) available: Estimated (scattering length) densities and volume fractions of molecular parts. Exemplary plot for a SAXS pattern recorded on a lab-instrument, for an X-ray wide scattering pattern, for a SANS Porod plot, and for the effect of SANS wavelength smearing. Additional scattering pattern simulations. See DOI: 10.1039/c0cp01201g

"quaternary amphiphile"[12] containing a long fluorocarbon chain (12 units) in addition to a hydrocarbon chain and two hydrophilic glycerol end groups. In this case, the demixing into nano-sized multi-compartments consisting of rods arranged in a Kagome tiling, was derived by electron-density reconstruction from the scattering pattern of a surface aligned sample. While this can be considered to be a polyphile, it is not a (thermotropic) star-polyphile, since it does not self-assemble to form three-phase lines, due to the linearly extended aromatic species, in contrast to the situation for star-polyphiles. The quaternary amphiphile assembles *via* hydrogen-bonding at either end of its extended aromatic core, forming walls rather than lines.

The possibility of forming three distinct domains and three-phase lines has been far better explored among the high-molecular weight analogues: star-shaped ABC "mikto-arm" block copolymers.[13,14] In contrast to the strong molecular incompatibility needed for small molecules discussed above,[15] segregation in copolymers can be achieved by minor chemical differences, whereby the degree of segregation is described by the term χN, where χ is the enthalpic Flory–Huggins inter-action parameter between the different blocks, and N is proportional to the molecular weight (entropic term). And in the case of polymers, the resulting multi-domains are large enough to be seen by electron microscopy. This has been a very active field of research: in dilute aqueous solution multi-compartment micelles were found,[16] and in the bulk a variety of novel multi-compartment structures were observed in experiments and simulations.[13,14] Depending on arm lengths, these mikto-arm star-polymers have been shown to form various cylindrical or prismatic structures, whose cross-sections transverse to the cylinder axes are planar tilings and even quasicrystals.[17] Other reported assemblies of these mikto-arm copolymers include spheres embedded in lamellae, striped cylinders, and most recently a 3D sphere packing into a zincblende structure.[18] Other observed morphologies seem to be more complex,[19] simulations suggest the potential for yet more complex structures.[20]

We are especially interested in the potential formation of network-like structures, where each domain (chemical species) forms an interpenetrating 3D periodic network, resulting in tri- or multi-continuous structures with multiple geometrically equivalent but chemically distinct networks, related to the now well-known bicontinuous cubic structures found in a variety of different systems ranging from surfactants and lipids to block copolymers and organelle membranes *in vivo*.[21–23] A hexa-gonal tricontinuous structure has been identified in a new mesoporous material templated by a novel surfactant,[24] but in that case all three channel systems are chemically equivalent. A simple theory of self-assembly of star-polyphiles suggests that tricontinuous structures should form for certain mole-cular shapes, particularly where the three arms of the star-shaped molecules are roughly equal in size ("balanced") and their is significant splay along each arm.[25]

We are attempting to form such tricontinuous structures in lyotropic mixtures of star-polyphiles in solution. Guided by our theoretical findings, we have synthesized comparatively simple star-polyphiles based on an aromatic center with attached hydrocarbon, fluorocarbon and methyl-capped oligoethylene-glycol chains (abbreviated H-chains, F-chains and O-chains), as shown in Fig. 1. These molecules form lyotropic liquid crystals in the presence of water. They can also be swollen with any or all of the solvents that mix with each arm (*e.g.* dodecane, F-nonane and water), often forming microemulsions.[26] SAXS patterns and phase behaviour suggest that many of these liquid crystalline structures are related to those found in conventional amphiphilic surfactant systems with bulky hydrophobic chains, raising the question if the hydrocarbon and fluorocarbon chains are in fact segregated, or if they combine to form one hydrophobic domain, making the star-polyphile effectively a double-chain surfactant. Our studies suggest significant differences.

In this contribution, we will focus on a single example: the hexagonal lyotropic mesophase which forms in a variety of star-polyphiles with different chain lengths. This is the dominant phase over a wide range of concentration and temperature. In addition, the corresponding amphiphilic double-chain surfactant forms a conventional hexagonal phase. To gain more insight into the underlying mesostructure, in addition to small-angle X-ray scattering data, we have done small-angle neutron scattering studies with contrast variation on selected star-polyphile hexagonal liquid crystals, and compare those data with data collected from the analogous hydrocarbon double-chain surfactant system. Unlike X-rays, the very different neutron scattering cross-sections between hydrogen and deuterium atoms allow us to highlight distinct fractions of the mesostructure, thereby effectively varying the contrast in the structure. We induce variable contrast by gradually replacing the H_2O by D_2O. (It should be noted that D_2O can slightly lower the phase transition temperatures, however this effect is negligible in the samples studied here.)[27]

The use of neutrons allows us to detect with accuracy the extent of mixing of the hydrocarbon and fluorocarbon chains. If they are completely mixed, then it is possible to contrast-match the resulting hydrophobic phase at the correct H_2O/D_2O ratio (the "matchpoint"), leading to (almost) zero scattering. In contrast, there is no such matchpoint if the hydrocarbons and fluorocarbons are spatially segregated. To quantify the extent of mixing, we use the total scattering of the sample, the so-called "Invariant" established by Porod.[28]
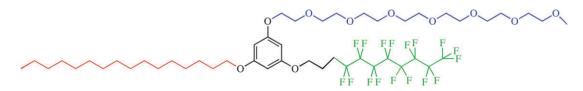

Fig. 1 Molecular structure of the star-polyphiles used in this study, abbreviated as B–O$_a$–H$_b$–F$_c$, where B denotes the aromatic molecular core, and O/H/F the methyl-capped oligoethyleneglycol, hydrocarbon and fluorocarbon chains of lengths a, b, and c respectively.

This journal is © the Owner Societies 2010

Finally, we also compare the experimental data at all measured contrasts to simulated scattering patterns based on the most likely model structures at the estimated experimental conditions.

Experimental section

Materials

A series of triphilic star-polyphiles and amphiphilic analogues were synthesised in our lab, *via* protocols to be published in detail elsewhere.[29] A brief summary of the synthetic route to star-polyphiles is the following. The three equivalent hydroxyl groups of 1,3,5 trihydroxybenzene precursors were first protected by tosylate groups, followed by sequential one-by-one hydrolysis in alkaline medium[30] and attachment of the respective arms *via* O-alkylation (Williamson reaction).

All molecules are star-shaped, with three oligomeric arms covalently linked to a central benzene ring (denoted "B"), as shown in Fig. 1. All molecules contained a single methyl-capped oligo-ethyleneglycol chain (denoted O_a, where "a" is the number of ethyleneoxide monomers). The surfactants contained in addition a pair of hydrocarbon aliphatic chains of length "b" (molecular species described as "$B–O_a–(H_b)_2$"). The triphilic star-polyphiles contain an oligo-ethyleneglycol chain, a single hydrocarbon chain and a single fluorocarbon aliphatic chain ("$B–O_a–H_b–F_c$"). The resulting molecules were >99% pure, as measured by mass spectroscopy. Here we report experimental results from the following molecules: $B–O_7–(H_{16})_2$, $B–O_7–H_{16}–F_{10}$ and $B–O_7–H_{14}–F_8$.

Mesophase formation in water

These molecular species were mixed with water in flooding experiments to ascertain the degree of liquid crystalline mesophase formation. Optical textures between crossed polarizers confirmed the presence of aqueous lyotropic mesophases for surfactants (as expected) as well as star-polyphiles (see Fig. 3). A suite of star-polyphile samples were prepared by mixing 0.200 g star-polyphiles with 50 μl ("25% samples") or 20 μl ("10% samples") of light and heavy water mixtures. The surfactant samples contained only 0.160 g surfactant, to give the same number of molecules (and roughly same volume fractions) as the corresponding star-polyphile samples, allowing for the much lower molecular weight of the surfactant than star-polyphiles (see Table S1, ESI‡). To promote water mixing and equilibration, the samples were melted with gentle heat in solvent-tight sample vials, vortexed and subsequently repeatedly centrifuged. They were then left to equilibrate for at least a week before scattering measurements. Between ≈25 and 35 °C for the surfactant and ≈30 to 42 °C for the star-polyphiles all samples were strongly birefringent, and showed fan-like textures, typical of conventional hexagonal mesophases.[31]

SAXS-setup

Preliminary SAXS scattering data were collected on a home-built Guinier apparatus to confirm sample equilibration (see Fig. S0, ESI‡). SAXS data were then collected on the SAXS beam-line at the Australian Synchrotron (Melbourne, Australia). The sample-detector distance was calibrated by collecting SAXS data on a known structural standard, silver behenate. All diffraction patterns were transmission-corrected and background subtracted. A home-built solvent-tight sample holder was used for the pastes. The cells were temperature controlled within 0.2 °C using a circulating water bath. The actual temperatures of the sample during measurement was checked by inserting a thermocouple into the bulky metal block containing the samples as close as practicable to the samples.

SANS-setup

SANS experiments reported here were performed with the SANS-1 instrument at the Paul Scherrer Institut (PSI), Switzerland. The experimental parameters for the experiments were chosen to maximize the accessible high q-range, covering q-ranges of $0.44\ \text{nm}^{-1} < q < 7.99\ \text{nm}^{-1}$. They were performed at a sample detector distance of 1.5 m, with the detector offset by 40 cm, a wavelength of 0.460 nm, and a primary beam collimation of 18 m. The wavelength resolution was 10% (full width at half-maximum value). The temperature controlled sample changer (MFU) with tight sample cells for solid samples, designed and provided by PSI, was used for all SANS-1 experiments.

BerSANS software (HMI, Berlin) was used for primary SANS data handling: the raw data were corrected for transmission, background from the sample cell and electronic noise; the two-dimensional scattering spectra were azimuthally averaged and corrected for detector efficiency, dividing them by the incoherent scattering spectrum of pure water; and finally the data were put on absolute scale using water as a secondary standard. For the determination of the scattering Invariant discussed below, we used the SAXSQuant Software package (Anton Paar, Graz).

Methods for SANS data evaluation

(i) Invariant. This parameter, established by Porod,[28,32] is a useful probe, particularly in the star-polyphile systems, to gain basic, model-independent information on samples from their scattering patterns. It corresponds to the total scattering of the sample, which is directly related to the volume fractions and squared scattering length density differences (SLDs) between the domains. It is therefore sensitive to the degree of segregation of various chemical species within the assemblies, while it is independent of the shape of the domains.

Fig. 2a shows the example of a 2-phase sample, in which the only contrast leading to scattering corresponds to the scattering length density difference between the droplets and the solvent. In that case, the theoretical Invariant Q_{th} can be calculated as
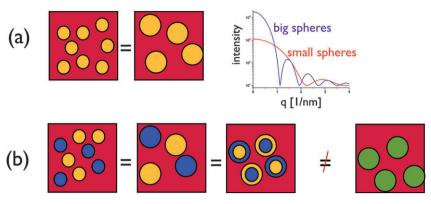
$$Q_{\text{th}} = 2\pi^2 \phi_1 \phi_2 (SLD_1 - SLD_2)^2$$

where ϕ_1 and ϕ_2 represent the volume fractions, and SLD_1 and SLD_2 the scattering length densities of the 2 phases.

For a multicomponent system, this equation can be generalized to

$$Q_{\text{th}} = 2\pi^2 \sum_i \phi_i (SLD_i - SLD_{\text{ave}})^2$$

where ϕ_i refers to the volume fraction of phase number i, and SLD_{ave} corresponds to the averaged scattering length density of the whole sample.

Fig. 2 The Invariant. (a) Two illustrative 2-phase systems, whose scattering spectra depend strongly on structural features in the sample. In contrast, the Invariant is independent of the model details depending only on the volume fractions and SLDs of the underlying domains. (b) Some 3-phase examples. Here the Invariant remains identical for the first three models, as the phases do not mix on a molecular scale. Mixing, resulting in a two-phase system (rightmost model), changes the Invariant.

Two things should be noted here: first, the SLD is assumed to be constant (homogenous) within each phase, and the interface between the phases is assumed to be well-defined and smooth, which in real samples is only an approximation. In practice, density and composition variations within a particular phase lead to variations of its SLD. Secondly, the volume fractions and SLD of each phase, required for the calculation of Q_{th}, are not exact, but estimated based on bulk densities (see Table S2, ESI‡).

Experimentally, the Invariant Q_{exp} can be determined from scattering curves via

$$Q_{exp} = \int I(q)q^2 dq$$

where $I(q)$ refers to the intensity in dependence of the scattering vector q. The experimental q-range needed for this integration, has to cover the dimensions of the underlying phases.

A schematic picture for a 3-phase system, of potential relevance to polyphilic systems, is shown in Fig. 2b. This shows that the Invariant Q is independent of the underlying structures, provided the 3 phases are separated into nano-sized domains. In contrast, if two of the chemical species mix on a molecular scale, they form a single nanometre-scale domain and the Invariant changes. Therefore, the Invariant is a very valuable tool for us to detect (de)mixing of the various molecular parts in the liquid crystalline structure.

A prerequisite for determining Q_{exp} accurately is to measure the whole small-angle range on absolute scale and up to high q-angles. In practice, both low and high q-values are experimentally inaccessible; the interpolations of q to 0 and to the high-angle limit were performed using the Guinier and Porod approximations respectively.[32] It should be noted that due to the q^2-dependence of Q_{exp}, the contribution from the Guinier-regime is negligible, while that of the Porod-regime is crucial. The Porod regime resolves the fine structural details, i.e., mostly the interfaces, and provided that these are well-defined and smooth, the intensity drops with q^{-4} (Porod law). This approximation can also be used for precise (incoherent) background determination, and a representative Porod plot for one our samples is shown in Fig. S1, ESI.‡ We note that the q^{-4}-behaviour observed over a wide q-range for all SANS samples

investigated, is in agreement with our assumption of well-defined, smooth interfaces between the different domains.

(ii) Numerical simulation of scattering patterns. In order to help identify the underlying structure from our scattering experiments, we simulated the scattering pattern for a range of candidate assemblies. These simulations were obtained by numerically computing the scattering pattern from digital (voxelised) models of realistic structures. We base these simulations on the Fourier transform (FT).
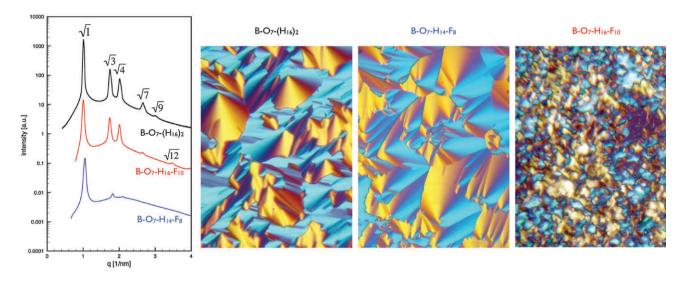
For monochromatic illumination, the scattering pattern observed from a given 3D structure can be modeled using the FT. There are various approaches to this. For example, the scattering pattern can be computed as the FT of the auto-correlation function of the scattering length density. This is well suited when the scattering length density is modeled as a random field, e.g., when the underlying structure exhibits random perturbations. Alternatively, the scattering intensity can be obtained as the FT of the structure itself. In order to get one dimensional "powder diffraction" patterns, in either approach, we need to average over all possible orientations of the structure. This is efficiently obtained by averaging the 3D FT over spherical shells to obtain a function which only depends on the magnitude of the q-vector.

Adopting the second approach, we have developed MPI-parallel (message passing interface) software for computing scattering patterns from large digital models. These simulations give the ability to study both the scattering peak locations and the relative magnitude of the peaks, thereby providing insight into the complex relationship between scattering length density distributions and scattering patterns which we observe in neutron contrast variation studies. Our tool represents an extension of the approach discussed in ref. 33, and will be published separately.[34]

Results & discussion

SAXS and polarising microscopy

Fig. 3 shows the synchrotron SAXS patterns for the 25% water samples containing B–O$_7$–(H$_{16}$)$_2$, B–O$_7$–H$_{16}$–F$_{10}$ and B–O$_7$–H$_{14}$–F$_8$. From ≈25 to 35 °C the surfactant, and

Fig. 3 Synchrotron SAXS patterns for the hexagonal liquid crystalline structure containing 25% water for the amphiphilic surfactant B–O_7–$(H_{16})_2$ at 30 °C, and the star-polyphiles B–O_7–H_{16}–F_{10} and B–O_7–H_{14}–F_8 at 35 °C. (The scattering curves are shifted by an arbitrary factor for clarity.) The microscopic textures between polarizers for all these hexagonal phases are typical fan-like patterns. B–O_7–$(H_{16})_2$ and B–O_7–H_{14}–F_8 liquid crystals were grown slowly in a water flooding experiment, while the B–O_7–H_{16}–F_{10} liquid crystal shown here resulted from re-crystallization from the melted state.

from ≈ 30 to 42 °C the star-polyphiles exhibit a lyotropic liquid crystalline phase that are consistent with 2D hexagonal symmetry (*p6mm*), evidenced by at least 3 peaks in the typical peak ratio of $\sqrt{1}\,\sqrt{3}\,\sqrt{4}\,\sqrt{7}\,\sqrt{9}\,\sqrt{12}...$[35] Neither SANS nor the high resolution SAXS data revealed scattering peaks other than those expected for this symmetry. Microscopy images for all these hexagonal phases showed fan-like textures, typical of conventional hexagonal mesophases, when grown slowly in a flooding experiment. The fans are less pronounced, when the hexagonal liquid crystal is obtained by re-crystallisation from the melt (B–O_7–H_{16}–F_{10} in Fig. 3).
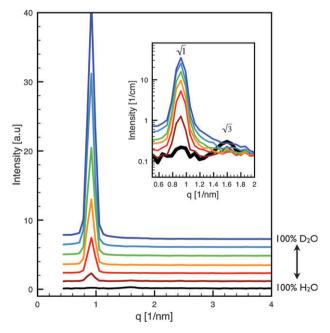
The underlying structure of B–O_7–$(H_{16})_2$ can be tentatively identified from the SAXS and optical texture data as a typical type-2 hexagonal phase, *i.e.*, a 2D-columnar phase that is composed of hydrophilic cylinders hexagonally arranged in a hydrophobic matrix.

Given the textural and SAXS data similarities between amphiphile and star-polyphile systems, the mesostructure of the star-polyphile samples appears to be related to the conventional hexagonal mesophase, with comparable unit cell dimensions to those formed in the conventional hexagonal mesophase. However, structural assignation on these bases alone for the star-polyphile systems is premature, as more detailed structural analyses—discussed below—reveal.
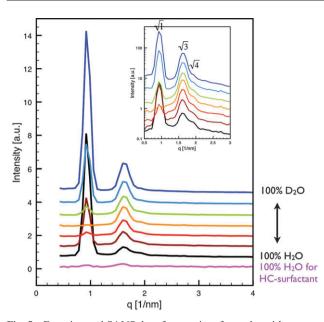
SANS data

A series of samples with increasing degrees of deuteration of the water solvent were prepared, to allow for varying neutron contrast, due to the distinct neutron scattering cross-section (scattering length density, or SLD) for H and D atoms. Separate samples of the amphiphile and star-polyphiles were mixed with 25 or 10% water, whereby the H_2O/D_2O wt/wt mixing ratios were 100/0, 80/20, 60/40, 50/50, 40/60, 20/80 and 0/100. It should be noted that in general the peaks observed by SANS are much broader than by SAXS due to overall limited

instrumental resolution, mostly from the 10% wavelength spread of neutrons and the detector resolution, but also from the collimation (see Fig. S3, ESI‡).

The SANS contrast variation data for the amphiphile samples B–O_7–$(H_{16})_2$ with 25% water at 30 °C are shown in Fig. 4. The sample containing pure H_2O gave rise to very little scattering, only marginally above background. As the relative content of D_2O increases, the intensity of the scattering

Fig. 4 SANS scattering data for a series of samples with neutron contrast variation of B–O_7–$(H_{16})_2$ with 25% water of varying H_2O/D_2O mixing ratios. (The scattering curves are shifted by an arbitrary factor for clarity.) Inset: magnified view of the peaks plotted with a logarithmic intensity scale.

Fig. 5 Experimental SANS data for a series of samples with neutron contrast variation for B–O_7–H_{16}–F_{10} with 25% water of varying H_2O/D_2O mixing ratios. Pink curve: B–O_7–$(H_{16})_2$ with 100% H_2O. This scattering pattern roughly corresponds to the contributed scattering from the aromatic centers, and a not fully homogenous hydrophilic phase. (The scattering patterns are shifted by an arbitrary factor for clarity.) Inset: magnified view of the peaks plotted with a logarithmic scale.
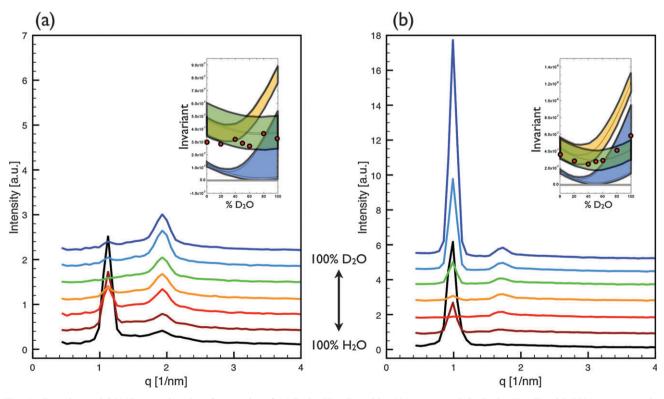
pattern grows also, with little variation in the shape of the SANS spectrum. Linear intensity *vs.* q plots reveal only a

single scattering peak. However, there is a subtle change in SANS spectra for D_2O-enriched samples, visible in logarithmic SANS plots (Fig. 4, inset).

The SANS contrast variation data for the star-polyphile samples B–O_7–H_{16}–F_{10} with 25% water at 35 °C are shown in Fig. 5. In contrast to the SANS data obtained from the amphiphilic system, both $\sqrt{1}$ and $\sqrt{3}$ peaks are visible for most samples. Indeed, the relative intensity of the $\sqrt{3}$ peak for the sample grows significantly as the proportion of D_2O/H_2O grows: at 50% D_2O, the $\sqrt{3}$ peak is significantly stronger than the (almost negligible) $\sqrt{1}$ peak; in addition, the third ($\sqrt{4}$) peak decreases (see logarithmic scale in inset). Most importantly, the overall intensity of the scattering data at all contrasts remains well above zero. This suggests that there are mesostructural differences between amphiphilic and star-polyphile hexagonal mesophases.

We have also measured the same contrast variation SANS series of B–O_7–H_{16}–F_{10} with a smaller hydrophilic volume fraction, by adding only 10% water. The results are shown in Fig. 6a. The trends for these samples mirror those found for the 25% water sample, namely reduction of the $\sqrt{1}$ peak and growth of the $\sqrt{3}$ peak with the degree of deuteration in the water. However, in contrast to above, the first peak does not increase again at the highest deuteration degree.

Lastly, we have collected SANS data from a deuteration series of hexagonal mesophases containing the star-polyphile B–O_7–H_{14}–F_8 with 25% water, shown in Fig. 6b. The trends observed in these samples are very similar as those found in B–O_7–H_{16}–F_{10} with 25% water above, albeit the second peak (the $\sqrt{3}$) is not as sharp.

Fig. 6 Experimental SANS scattering data for a series of (a) B–O_7–H_{16}–F_{10} with 10% water, and (b) B–O_7–H_{14}–F_8 with 25% water samples measured at 35 °C with of varying H_2O/D_2O mixing ratios. Inset: Comparison between experimental and theoretical Invariant as describe in Figure caption 11.

Structural analysis

B–O$_7$–(H$_{16}$)$_2$ amphiphile hexagonal phase. A schematic view of the expected SANS scattering for a "deuteration series" of samples with identical water–amphiphile contents and varying deuterium content in the water is schematically illustrated in Fig. 7. Quantitative estimation of the scattering power as a function of deuterium content is done by calculating the scattering length densities (SLDs) and volume fractions of individual domains in each sample, based on their bulk densities (see ESI‡). The SLD differences between domains ("contrast") give rise to scattering, whereby the total scattered intensity (Invariant) is proportional to the squared contrast and the volume fractions involved (see Methods). Assuming these amphiphilic systems form mesostructures containing only two distinct domain types, namely hydrophobic (red) and hydrophilic (blue) domains, the deuteration series have uniform SLDs, regardless of the degree of deuteration, coloured in Fig. 7 from yellow to brown. At 100% H$_2$O, the two SLDs would be equal (matchpoint), and thus there is no contrast in the system, and no scattering. Increasing the D$_2$O/H$_2$O ratio should increase the total scattering, due to the enhanced contrast between the hydrogenated hydrophobic domain, and the more deuterated hydrophilic domain. However, the shape of the scattering curves is expected to remain unchanged, since the underlying structure remains unchanged.

Overall, this behaviour is in good agreement with the experimental data on the B–O$_7$–(H$_{16}$)$_2$ system, shown in Fig. 4: there is almost no scattering at 100% H$_2$O, and then the intensity of the scattering curve increases at almost constant shape (on a linear scale, only the first order hexagonal peak is visible). However, there is a small but significant change in shape, which can be better seen when looking at the scattering curves on a logarithmic scale (inset). The effect is small, but in fact, at 100% H$_2$O the second peak has higher intensity than the (vanished) first peak, which is inconsistent with a true 2-phase system as discussed above, and has to be attributed to the presence of a third phase, or SLD-variations within a phase. We therefore constructed a series of structural models with varying degrees of chemical segregation within the mesostructures, as shown on top of Fig. 8.

(a) Two distinct domains: one hydrophilic containing all water and oligo-ethyleneglycol fractions and the hydrophobic domains enclosing all hydrocarbon molecules.

(b) Three distinct domains, identical to the previous model, with the addition of a sheath of aromatic component of uniform thickness surrounding all hydrophilic cylinders, corresponding to the star-molecular cores.
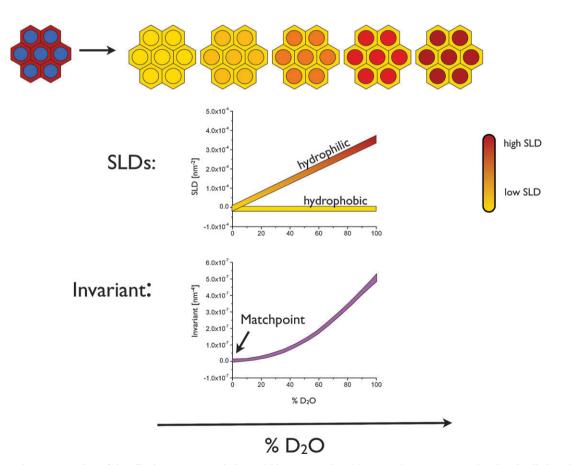

Fig. 7 Schematic representation of the effective contrast variations within a conventional hexagonal mesostructure showing the distinct domains with varying scattering length densities (SLD) (coloured from yellow to brown) for B–O$_7$–(H$_{16}$)$_2$ with 25% water. The different contrasts along the SANS contrast variation line mimic the effect of replacing H$_2$O increasingly by D$_2$O. Quantitative estimates of the estimated SLDs and Invariants are plotted as a function of the D$_2$O content.

(c) Three distinct domains, identical to model (a), but the hydrophilic domains are fractionated into oligo-ethyleneglycol moieties (of uniform thickness) and bulk water.

(d) Four distinct domains, identical to model (c), with the addition of a separate aromatic sheath, as in model (b).

For convenience, these hexagonally-packed columns are assumed to have hexagonal polygonal cross-sections. In practice, their shape is likely to be somewhat rounded, but this effect changes little the detailed conclusions, although scattering is sensitive to this geometry (see Fig. S4, ESI‡). The domain volume fractions and SLDs are based on estimates from the bulk (see Table S2, ESI‡).

These models give rise to the simulated scattering patterns shown in Fig. 8. These simulations confirm that the (dis)appearance of peaks is not related to systematic extinctions within the liquid crystal symmetry, but is rather due to subtle variations of the form factor of the underlying structures. These changes in the underlying structure evidently cause the form factor minima to move, thereby varying the relative intensities of the $\sqrt{1}$ and $\sqrt{3}$ peaks considerably. Indeed, simulations of all four structural models (a–d above) reproduce the essential features of the experimental data: the first peak is dominant and strongly increases on substitution of D for H in the aqueous solvent. Model (b) also admits the possibility of a more intense $\sqrt{3}$ peak than the $\sqrt{1}$ peak (Fig. 4, inset); *i.e.*, the presence of a separated aromatic domain can induce this effect (Fig. 8b), while a distinct bulk water domain alone cannot (Fig. 8c).
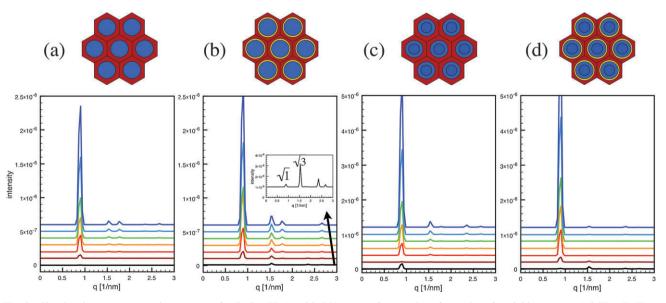
Closer inspection of the experimental SANS spectral variations through the deuteration series reveals more subtle variations of the $\sqrt{3}$ peak. Though conclusive data are difficult to obtain here, it appears that the $\sqrt{3}$ peak decreases, and then either stays very small or increases slightly again on increasing the degree of deuteration. This feature cannot be reproduced in simulations by model (b) alone (Fig. 8b). However, it can be

reproduced if we allow for variations in the scattering contrast within the hydrophilic phase. The case of complete demixing within the hydrophilic domains is that of model (d). Fig. 8d depicts the expected scattering within this scenario, which assumes total phase separation of water molecules from oligo-ethyleneglycol chains. But in fact, assuming partial demixing of only 5 vol% of separated water is already sufficient to find good agreement between simulated scattering spectra and recorded data (see Fig. S4d, ESI‡).
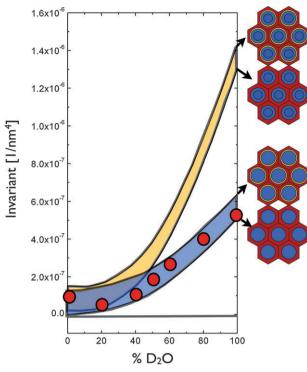
We use measured values of the Invariant to probe further the degree of domain segregation within this mesophase. Fig. 9 shows the trend of the experimental Invariant, Q_{exp}, compared to the theoretical Invariants (Q_{th}) for the four models (a–d), as estimated from bulk densities (see Table S2, ESI‡). The blue region corresponds to a homogeneous hydrophilic phase, whereas the yellow region corresponds to complete separation of water and oligo-ethyleneglycol chains. Theoretical Invariants have been estimated assuming a continuum of models with varying segregation of the aromatic cores. The upper bound for each band corresponds to a complete separation of the center, while the lower bound corresponds to perfect mixing of the cores with the hydrocarbon chains.

The experimental data lie squarely within the blue region, suggesting that the hydrophilic phase is rather homogenous. This excludes the model (c) and (d) based on strong demixing of oligo-ethyleneglycol with water discussed above, but we cannot exclude a slight demixing. Further, there is no significant tendency towards either bound on Q, suggesting that the aromatic cores may be either (partially) mixed or segregated into a separate domain. A more detailed interpretation is restricted due to uncertainties stemming from the assumed sharp interfaces, constant SLDs within each phase and estimated volume fractions.

In summary, this amphiphilic system is essentially a hydrophilic/hydrophobic 2-phase system, with minor

Fig. 8 Simulated neutron scattering patterns for B–O$_7$–(H$_{16}$)$_2$ with 25% water for a series of samples of variable contrast (*cf*. Fig. 5). Four theoretical models occur, illustrated schematically: (a) a hydrophilic/hydrophobic 2-phase system (with miscible H-chains and aromatic cores, as well as O-chains and water), (b) model (a) with spatially segregated aromatic cores, (c) model (a) with demixed O-chains and water, and (d) four-phase model consisting of spatially segregated aromatic cores as well as O-chains and water.

Fig. 9 Comparison of theoretical and experimental scattering Invariants, Q_{th} (yellow and blue bands) and Q_{exp} (red circles) for mesophases containing B–O$_7$–(H$_{16}$)$_2$ with 25% water. Blue band: theoretical invariants assuming a homogenous hydrophilic domain; upper and lower bounds assuming two- or three-phase segregation according to structural models illustrated at right (*cf*. Fig. 8). Yellow band: spatial segregation of water and O-chains; bounds set by limiting structural models illustrated at right (*cf*. Fig. 8).

additional SLD-inhomogeneities, probably due to a partially separated center in combination with slight demixing in the hydrophilic domain. The data are in good agreement with the expected structure of hydrophilic rods arranged hexagonally in a hydrocarbon matrix.

B–O$_7$–H$_{16}$–F$_{10}$ and B–O$_7$–H$_{14}$–F$_8$ star-polyphile hexagonal mesophases. Candidate hexagonal mesostructures for the star-polyphile–water mixtures are potentially more complex than their amphiphilic counterparts, due to presence of the fluorocarbon in addition to hydrocarbon chains. Nanoscale segregation of the fluorocarbon and hydrocarbon species would lead to an additional domain type, with distinct scattering length density in SANS experiments.

Fig. 10 illustrates a qualitative view of the contrast variations according to two distinct scenarios that are feasible for the star-polyphile–water samples containing 25% water. In the first scenario, the H-chains and F-chains mix homogeneously (bottom of figure), and the system resembles closely the 2-phase system (hydrophilic/hydrophobic), discussed above. But in contrast to the surfactant case, the SLDs of the 2 phases are matched in the middle of the contrast variation line (zero scattering) and not at 100% H$_2$O, because the SLD of fluorocarbons is quite high (comparable to deuterated materials). In the second scenario, the H-chains and F-chains are spatially segregated (top of figure), giving a true 3-phase system (hydrophilic, oleophilic and fluorophilic).

At 100% H$_2$O, the SLD of the hydrophilic domain would match that of the H-chains, and the scattering would mostly stem from the F-chains. At 100% D$_2$O, the case is reversed: the SLD of the hydrophilic domain would match that of the F-chains, and the scattering would mostly stem from the H-chains. In the middle of the contrast variation line, there is a slight minimum of the total scattering (as shown by the Invariant in Fig. 10). However, unlike the 2-phase system, there is no overall matchpoint, as it is obviously impossible in such a 3-phase system to match all contrasts simultaneously.

The plot of the experimental data for B–H$_{16}$–F$_{10}$–O$_7$ (Fig. 5), also includes the (pink) scattering curve of the B–O$_7$–(H$_{16}$)$_2$ at the matchpoint, corresponding to the maximum scattering contribution stemming from the SLD-inhomogeneities discussed above for the amphiphilic system. This curve can be compared to the suspected matchpoint for a potential 2-phase system for the star-polyphile (orange line). It is very clear that the observed intensity is much higher for the star-polyphiles than can be explained assuming nanoscale mixing of the various potentially mutually miscible chemical moieties.

Quantitative comparison between the experimental and theoretical total scattering (Invariants) is shown in Fig. 11. Theoretical values of Q_{th} are again estimated based on the bulk densities of the system (see Table S2, ESI‡), and are plotted with a range of possible values, depending on various possible mixing scenarios. Several scenarios are chemically possible, depending on whether the H-chains and F-chains mix, whether the oligo-ethyleneglycol chains and water mix, whether the center and the H-chains mix, and whether the C$_3$-spacer between the center and the F-chains in the star-polyphile molecules can itself form a segregated phase (see Fig. 1). Fig. 11 shows that expected values of the Invariant Q_{th} fall into 3 main regions: mixing of the fluorocarbon and hydrocarbon species (blue region), spatial segregation of the fluorocarbon and hydrocarbon species and mixing of oligo-ethyleneglycol chains with water (green region), and segregation of the fluorocarbon and hydrocarbon species as well as the oligo-ethyleneglycol chains and water (yellow region). The experimental Invariant data, Q_{exp}, lie within the green region, indicating that the oligo-ethyleneglycol chains form a rather homogenous mixture with the water, while the fluorocarbon and hydrocarbon species form segregated domains.

Note that the star-polyphile molecular architecture implies that self-assembly of star-polyphiles without hydrocarbon-fluorocarbon mixing and with the usual hydrophilic-hydrophobic segregation, common to amphiphiles, must result in patterns containing fluorocarbon–hydrocarbon, hydrocarbon–hydrophilic and hydrophilic–fluorocarbon interfaces. Further, since these three domains within each star-shaped star-polyphile molecule share a common (aromatic) centre, all three interfaces necessarily meet along three-phase lines, as in a (vertex-free) topological foam. The simplest structure that is consistent with these requirements and the 2D hexagonal (*p6mm*) symmetry inferred from the scattering peak positions is a hexagonal honeycomb pattern, which is the usual mesostructure of surfactant hexagonal mesophases, albeit decorated with three distinct domain types or "colours" (Fig. 12a, inset). For convenience, we describe this pattern by
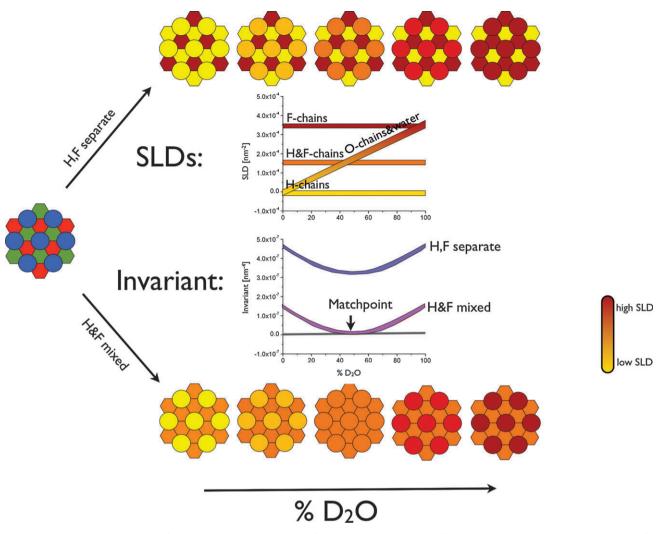
Fig. 10 Schematic representation of the contrast (yellow to brown) for neutron scattering according to calculated scattering length densities for chemically distinct domains—for star-polyphiles with 25% water along the contrast variation line formed by replacing H_2O increasingly by D_2O. Also shown are the estimated SLDs and Invariants. Lower models show the contrast assuming miscibility of the H-and F-chains, forming a homogeneous hydrophobic phase (orange). Within this model, an overall matchpoint (with zero scattering) is expected in the middle of the contrast variation line. The upper models assume complete spatial segregation of the H-and F-chains. In this scenario, only the F-chains are visible at 100% H_2O, and only the H-chains are visible at 100% D_2O; in the middle of the contrast variation line, the invariant has a minimum, but it remains far from zero.
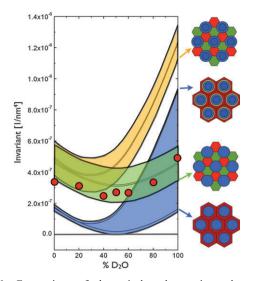
the planar tiling of an orthogonal cross-section. Since this tiling is the usual tiling by hexagons, we denote it the 6.6.6-tiling, as each of the three phases have six neighbors. However, an infinite sequence of three-coloured *p6mm* tilings of the plane can be constructed, where all vertices are common to three cells, one of each colour. These are formed by changing systematically the polygonal shape of tiles of one colour at the expense of the other two tile types. The next simplest tiling of hexagonal symmetry beyond the 6.6.6-tiling is the 12.6.4-tiling. The latter planar pattern results in a 3D mesostructure with dodecagonal prismatic domains of one colour, surrounded by hexagonal and quad-rangular prisms of the other two colours (Fig. 12b, inset). Because the sample under investigation has a rather large hydrophilic volume fraction (O/H/F $\approx$ 46/22/25, and ≈ 7 for the center), we assume that the larger dodecagonal prisms contain the hydrophilic fractions of the hexagonal

mesophase, and two models can be built from this pattern: one containing hydrocarbon-filled hexagonal prisms and fluorocarbon-filled quandrangular prisms, and another with the converse filling.

These therefore give rise to three distinct structural models analogous to those for the amphiphilic system, but accounting for the distinct fluorocarbon and hydrocarbon domains (see insets of Fig. 12):

(a) Three distinct domains, whose idealised shapes are all hexagonal prisms, constructed from the 6.6.6-tiling. The hydrophilic domain contains the oligo-ethyleneglycol moieties and bulk water; the other two domains are filled with hydro-carbon and fluorocarbon respectively.

(b) Three distinct domains, constructed from the 12.6.4-tiling, with hydrocarbon moieties within the hexagonal prismatic domains and fluorocarbon moieties within the quadrangular domains.

Fig. 11 Comparison of theoretical and experimental scattering Invariants, Q_{th} (yellow, green and blue bands) and Q_{exp} (red circles) for B–O_7–H_{16}–F_{10} with 25% water. Blue band: expected invariants assuming complete miscibility of F-and H-chains; the lower bound corresponds to full mixing of water/O-chains and centers/H-chains, respectively, while these are assumed to be four spatially separate phases at the upper bound. Green band: expected invariants assuming spatial segregation of F- and H-chains and miscibility of O-chains and water. Yellow band: expected invariants assuming spatial segregation of both F- and H-chains and O-chains and water. The lower bound in the green and yellow region corresponds to full mixing of centers/H-chains, and C_3-spacer/F-chains, respectively, while these are assumed to be four spatially separate phases at the upper bound.
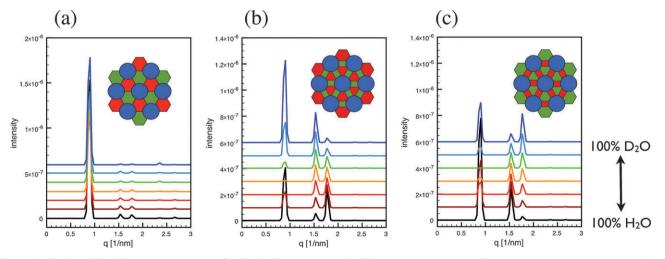
(c) Three distinct domains, constructed from the 12.6.4-tiling, with hydrocarbon and fluorocarbon moieties within the quadrangular and hexagonal prismatic domains respectively.

For convenience, we have assumed that all the interfaces are flat, so that the 2D tilings contain straight edges only. The structural dimensions of each model pattern have been calculated based on volume fractions of each domain (see Table S2, ESI‡ whereby the volumes of center/H-chain, C_3-spacer/F-chain,

and water/O-chains were combined). Note that small variations of volume fractions such as the precise fractionation of the aromatic cores between each of the three domains do not influence our conclusions (see Fig. S5, ESI‡).
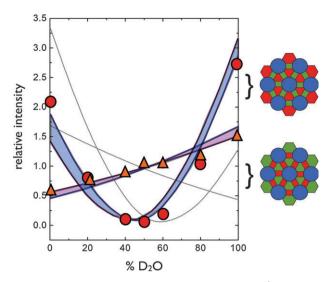
Fig. 12a shows the simulated scattering curves for model (a), calculated for a series of samples with varying deuterium fractions within the water. Simulated SANS scattering spectra from these structural models fail to reproduce the experimental results. For example, the simulated data give a $\sqrt{1}$ peak well above zero along the entire deuteration series, and the second peak remains less intense than the first, irrespective of the degree of deuteration. Indeed, this feature is a basic feature of this conventional hexagonal mesostructural model. For instance, scattering simulations of model structures far removed from the experimental conditions nevertheless exhibit a far more intense $\sqrt{1}$ peak than $\sqrt{3}$ peak (see Fig. S8 and S9, ESI‡). On that basis, we confidently exclude model (a)—the decorated conventional hexagonal phase mesostructure—as a possible model for all of the investigated hexagonal mesophases of these star-polyphile–water systems.

In contrast to the poor fit between expected scattering from model (a) and experimental data, simulations of models (b), based on a 12.6.4-tiling, reproduce the experimentally observed features well. For example, model (b) results in a reduction of the $\sqrt{1}$ peak to zero intensity with partial substitution of deuterium for hydrogen, accompanied by an increase in the intensity of the $\sqrt{3}$ peak, while the $\sqrt{4}$ peak decreases, as shown in Fig. 12b. We note, however, that this behaviour is not found in model (c), where the H-chains and F-chains fill quadrangular and hexagonal prismatic domains respectively. In those cases, simulations show that the relative intensity of the $\sqrt{3}$ peak decreases on deuteration of the water solvent (see Fig. 12c).

The agreement between model (b) and the experimental data is robust. For example, small variations in the volume fractions or SLDs (resulting e.g., by introducing a phase-separated aromatic domain) do not have a strong impact on the observed trend (see Fig. S5, ESI‡). The scattering patterns that result by varying the assignment of various volume

Fig. 12 Simulated SANS scattering patterns for B–O_7–H_{16}–F_{10} star-polyphile samples containing 25% water assuming (a) an underlying 6.6.6-tiling, (b) an underlying 12.6.4-tiling, with the hydrocarbon chains filling the hexagons and fluorocarbon chains filling the quadrangles, and (c) an underlying 12.6.4-tiling, with the fluorocarbon chains filling the hexagons and the hydrocarbon chains filling the quadrangles.

Fig. 13 Comparison of normalised intensity of the $\sqrt{1}$ peak and $\sqrt{3}$ peak in the star-polyphile sample B–O$_7$–H$_{16}$–F$_{10}$ samples mixed with 25% water. Experimental data: $\sqrt{1}$ peak: red circles, $\sqrt{3}$: orange triangles. Simulations based on the 12.6.4. tiling of model (b) of Fig. 12: $\sqrt{1}$ peak: blue band, $\sqrt{3}$: purple band. The width of the band represents the effect of a (partially) separated aromatic center. Simulations based on the 12.6.4 tiling of model (c) of Fig. 12: grey lines.

fractions to each of the three domain types are shown in Fig. S6 and S7, ESI.‡

A quantitative comparison between simulations of model (b) and the experimental data is given in Fig. 13, that compares the normalised intensities of the $\sqrt{1}$ and $\sqrt{3}$ peaks, respectively, *i.e.*, each peak is normalised by the average intensity of this peak within the contrast variation series. The simulated normalised peak intensities are plotted as a band whose width spans the extremes of total segregation of the aromatic core from all other domains and miscibility with the hydrocarbon domains. The agreement between model (b) and the experiments is remarkable. The grey lines denote these two peak intensities for model (c), and clearly do not fit the experimental data. We note that in the simulated data, the $\sqrt{3} : \sqrt{1}$ peak intensity ratio is higher than in the experimental data. We attribute this to thermal motions and the experimental neutron wavelength-spread, which are not included in the simulations (see Fig. S3 ESI‡).

The disappearance of the $\sqrt{1}$ peak and enhanced $\sqrt{3}$ peak were also observed in the experimental contrast variation data for B–O$_7$–H$_{16}$–F$_{10}$ hexagonal mesophases containing only 10% water, suggesting the same underlying structure. In contrast to the 25% water samples, the variation with deuteration is somewhat diminished due to the lower water content, and the 10% sample with pure D$_2$O exhibits a similar scattering pattern and Invariant as the 25% water sample with equal fractions of H$_2$O and D$_2$O (see Fig. 9). Again, Q_{exp} lies in the green region of Q_{th} (see Fig. 6a inset), indicating that the fluorocarbon and hydrocarbon species form segregated domains for these dryer mesophases also.

Our data prove that the presence of 10 perfluoroalkyl-units in the fluorocarbon chains forces them to demix from the hexadecanyl hydrocarbon chains, over a range of water contents. Can we expect the same behaviour for samples containing shorter fluorocarbon chains in hexagonal meso-phases of the B–O$_7$–H$_{14}$–F$_8$ star-polyphile with 25% water, containing only 8 perfluoroalkyl-units? In fact, the SANS data reveal that the fluorocarbon and hydrocarbon chains remain strongly spatially segregated in these cases also: the measured Invariants, Q_{exp} again lie within the theoretical range predicted for segregation (Fig. 6b, inset). However, the asymmetry of the experimental values (Q_{exp} at 100% D$_2$O slightly above green region), indicating SLD-variations in the hydrophilic region, seems a little more pronounced than in the B–O$_7$–H$_{16}$–F$_{10}$ samples. But again the trend in the experimental contrast variation data mirror those discussed above, suggesting the same mesostructure based on the 12.6.4-tiling. The $\sqrt{3}$ peak along the whole contrast variation series is less pronounced than in B–O$_7$–H$_{16}$–F$_{10}$. This was already observed in the corresponding SAXS data (Fig. 3), and indicates more order in the liquid crystals with the longer chains.
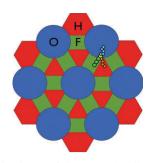
Discussion and conclusions

The amphiphilic system is essentially a 2-phase system, with minor additional SLD-inhomogeneities, probably due to a partially separated center in combination with slight demixing in the hydrophilic domain. The data are in very good agreement with the structure of a type-2 hexagonal phase.

As mentioned above, the deviations from a pure 2-phase system in the amphiphilic system are small and should not be over-interpreted. However, from a physicochemical point of view, these deviations make sense. It is very unlikely that the aromatic centers are completely mixed with the hydrophobic chains, as the star-molecular architecture ensures that aromatic species are concentrated at the interface between hydrophilic and hydrophobic domains. Complete segregation, on the other hand would be expected for example if the aromatic centres are co-localised by π–π-stacking interactions, as seen in related molecules.[36] However, a single benzene ring alone is unlikely to induce sufficiently strong interactions; indeed, we find no evidence for the presence of these inter-actions. For example, we did not detect wide-angle scattering (WAXS) peaks indicative of ordering between adjacent benzene cores (see Fig. S2, ESI‡).

The dimensions of the hydrophilic channels estimated from the SAXS data support our finding of slight segregation within the hydrophilic domains. The B–O$_7$–(H$_{16}$)$_2$ amphiphile hexa-gonal phase has a unit cell dimension of 7.7 nm, and with 46% v/v hydrophilic domain, the hydrophilic channel radius is estimated to be 2.7 nm. While oligoethylene-glycol and water are known to mix very well, the fully stretched length of heptaethylene-glycol is estimated to be only about 2.5 nm,[37] thus demanding a film of bulk water within these domains.

In contrast, SANS data for the star-polyphiles offer clear evidence that these systems are effectively segregated into three distinct domains at the mesoscale with spatially distinct hydrophilic, oleophilic and fluorophilic domains (with minor additional SLD-inhomogeneities). The simplest hexagonal mesostructure consistent with the molecular star-architecture, and in very good agreement with the experimental data, is a hexagonal arrangement of infinite columns whose cross-section is the planar 12.6.4-tiling. Our analysis suggests that

Fig. 14 Schematic picture of the star-polyphile molecular arrangement in the 12.6.4 tiling found for the star-polyphile hexagonal mesophases. The dimensions of the green fluorocarbon domains compared with the molecular dimensions requires some interdigitation of fluorocarbon chains.

the hydrophilic domain fills the large dodecagonal prismatic domains, the hydrocarbon chains the hexagonal prisms and the fluorocarbon chains the quadrangular prisms.

From a molecular point of view, it is not surprising that the fluorocarbons line the quadrangular domains. Fluorocarbon chains are far stiffer than hydrocarbons,[6] mostly due to the larger volume requirement of F- *vs.* H-atoms, with a strong preference for unsplayed chain packings, favouring their location at interfaces with low curvatures. Indeed, comparison of fluoro- and hydrocarbon surfactants with similar headgroups shows that fluorocarbon surfactants generally form locally flat interfaces (lamellae, vesicles), while their hydrocarbon analogues form more curved structures. Due to their rectangular cross-section, a locally parallel array of fluorocarbon chains is readily realised in the quadrangular prisms; further the more flexible H-chains can more readily fill the hexagonal domains, which require enhanced molecular splay.[35,38] In addition the F-chains are shorter, as they have been designed to have the same volume as the H-chains, but they have a much larger cross section.[6] This is schematically shown in Fig. 14.

While the 12.6.4-tiling has not been recorded in lyotropic liquid crystals until now, columnar domains based on a variety of Archimedean tilings have been observed in the polymeric analogues of star-polyphiles[13,14] as well as simulations of star-polyphiles and polymers.[39,40] In the case of ABC mikto-arm copolymers, the particular tiling that gives rise to a columnar phase depends on the relative volume of the three chains. Monte Carlo simulations of three-arm star-shaped molecules detect the 12.6.4.-tiling for a ratio of chain volumes of $2:1:1$,[40] which is in good agreement with the volume fraction of chains in our 25% water star-polyphile samples (O/H/F $\approx 46/22/25$, and $\approx 7\%$ occupied by the aromatic core "B" for B–O$_7$–H$_{16}$–F$_{10}$). According to simulations, distinct tiling patterns emerge. For example, as the chains approach equal volume fractions (and the molecules become increasingly balanced), the tiling changes from 12.6.4. *via* intermediate patterns to the 6.6.6 tiling, assuming that all interactions between unlike chains are of equal strength.[39] More balanced star-polyphile–water mixtures can be formed by reducing the hydrophilic volume from 25% water. However, the star-polyphile samples containing only 10% water - at estimated volumes of O/H/F $\approx 36/25/30$ (and ≈ 9 for the core) also

exhibit this novel hexagonal mesostructure, based on the 12.6.4-tiling. Clearly, then, star-polyphile lyotropic phase behaviour is not identical to that of copolymers.

This distinction between star-polyphile and mikto-arm copolymer self-assembly is significant. It indicates that volume is not the only factor determining the mesostructure in star-polyphile systems, whose ultimate structures result from a delicate balance of many factors. In particular, we suspect the following features of our current suite of star-polyphiles influences their phase behaviour.

First, as noted above, steric issues arising from packing of fluorocarbon chains favour the fluorocarbon packing within quadrangular prismatic domains. The 12.6.4. tiling is the only known three-coloured planar tiling where fluorocarbon domains occupy only 4-sided prismatic domains. All other known 3-coloured (*p6mm* symmetry) patterns based on Platonic or Archimedean tilings contain domains of one colour with both 4- and 6-sided polygons, implying that fluorocarbons are then forced to occupy both (favoured) quadrangular prismatic and (disfavoured) hexagonal prismatic domains.

Secondly, the surface tension between the fluoro- and hydrocarbon domains is much weaker than the surface tensions acting between adjacent (fluoro- or hydro-carbon) oil-filled domains and the hydrophilic domains. This effect allows the interfaces to relax from foam-like geometries, favoured for equal surface tensions between all three interface types. Thus, it can be advantageous to increase the H/F interface by making the neighbouring H-domains and F-domains smaller, if this means that the hydrophilic/hydrophobic interface can be minimized and better covered by the aromatic centers. In the 12.6.4. tiling, the aromatic centers can spread most evenly at the hydrophilic/hydrophobic interface.

This novel hexagonal mesostructure based on the 12.6.4-tiling pattern exists over a broad range of water content—at least between 10–25% (corresponding to an estimated hydrophilic volume fraction of 36–46%). In addition, it forms in star-polyphile systems with shorter hydrocarbon and fluorocarbon chains, where *a priori* one may predict formation of the more conventional two-phase hexagonal mesostructure. The mixing behavior of hydrocarbons with fluorocarbons is well established to be non-ideal,[6,7] and in general eight perfluoroalkyl units are considered to be the critical requirement to cause hydrocarbon/fluorocarbon phase segregation at room temperature, based on studies of liquid–liquid mixtures of hydrocarbon and fluorocarbon amphiphilic molecules.[41] However, studies of mixed hydrocarbon and fluorocarbon surfactants in solution show that this demixing cannot be taken for granted. Not only does it depend on temperature and the length of the respective hydrocarbon and fluorocarbon chains, but also on the type of hydrophilic headgroup involved.[10,42] Systematic studies of ternary phase diagrams based on nonionic hydrocarbon and fluorocarbon amphiphile–water mixtures show that a single type-1 hexagonal phase is formed for all ratios of hydrocarbon (with 12 CH$_2$ units) and fluorocarbon surfactants (with 8 CF$_2$ units), suggesting full molecular miscibility in this case.[43] Given those findings, and the added constraint that fluoro- and hydrocarbon chains are

intimately adjacent in star-polyphiles due to a common aromatic centre, it is reasonable to expect miscibility of fluorocarbon and hydrocarbon species in star-polyphile lyotropic mixtures. Recall, however, that the SANS data give unequivocal evidence that the fluorocarbon and hydrocarbon species have not become significantly more miscible upon reducing the fluorocarbon chainlength to 8 units: the scattering Invariant clearly adopts a value corresponding to that expected for spatially segregated hydrocarbon and fluorocarbon nanoscale domains (Fig. 6b, inset).

Finally, it should be noted that other novel lyotropic mesophases have also been found in these star-polyphile systems. Their mesostructures will be reported in later papers. We are confident that this new class of molecules will display at least the mesostructural wealth that has been reported over past decades in lyotropic surfactant systems.

Acknowledgements

References

1 G. J. T. Tiddy, *Phys. Rep.*, 1980, **57**, 1.
2 S. Trabelsi, S. Zhang, T. R. Lee and D. K. Schwartz, *Phys. Rev. Lett.*, 2008, **100**, 037802.
3 W. Guo, L. Zhong, B. M. Fung, E. A. Orear and J. H. Harwell, *J. Phys. Chem.*, 1992, **96**, 6738.
4 Y. Kondo and N. Yoshino, *Curr. Opin. Colloid Interface Sci.*, 2005, **10**, 88.
5 A. Ohno, A. Kushiyama, Y. Kondo, T. Teranaka and N. Yoshino, *J. Fluorine Chem.*, 2008, **129**, 577.
6 M. P. Krafft and J. G. Riess, *Chem. Rev.*, 2009, **109**, 1714.
7 M. P. Krafft, *Adv. Drug Delivery Rev.*, 2001, **47**, 209.
8 M. Sanchez-Dominguez, N. Benoit and M. P. Krafft, *Tetrahedron*, 2008, **64**, 522.
9 A. Dupont, J. Eastoe and L. Martin, *Langmuir*, 2004, **20**, 9960.
10 M. Almgren, V. M. Garamus, L. Nordstierna, J. Luc-Blin and M. J. Stebe, *Langmuir*, 2010, **26**, 5355.
11 C. Tschierske, *Chem. Soc. Rev.*, 2007, **36**, 1930.
12 B. Glettner, F. Liu, X. B. Zeng, M. Prehm, U. Baumeister, M. Walker, M. A. Bates, P. Boesecke, G. Ungar and C. Tschierske, *Angew. Chem., Int. Ed.*, 2008, **47**, 9063.
13 N. Hadjichristidis, H. Iatrou, M. Pitsikalis, S. Pispas and A. Avgeropoulos, *Prog. Polym. Sci.*, 2005, **30**, 725.
14 Y. Matsushita, A. Takano, K. Hayashida, T. Asari and A. Noro, *Polymer*, 2009, **50**, 2191.
15 C. Tschierske, *Curr. Opin. Colloid Interface Sci.*, 2002, **7**, 355.
16 Z. B. Li, E. Kesselman, Y. Talmon, M. A. Hillmyer and T. P. Lodge, *Science*, 2004, **306**, 98.
17 K. Hayashida, T. Dotera, A. Takano and Y. Matsushita, *Phys. Rev. Lett.*, 2007, **98**, 195502.
18 K. Hayashida, A. Takano, T. Dotera and Y. Matsushita, *Macromolecules*, 2008, **41**, 6269.
19 S. Okamoto, H. Hasegawa, T. Hashimoto, T. Fujimoto, H. M. Zhang, T. Kazama, A. Takano and Y. Isono, *Polymer*, 1997, **38**, 5275.
20 J. J. K. Kirkensgaard and S. Hyde, *Phys. Chem. Chem. Phys.*, 2009, **11**, 2016.
21 S. T. Hyde, S. Andersson, Z. Blum, S. Lidin, K. Larsson, T. Landh and B. W. Ninham, *The Language of Shape*, Elsevier Science B.V, Amsterdam, 1997.
22 H. Jinnai, Y. Nishikawa, R. J. Spontak, S. D. Smith, D. A. Agard and T. Hashimoto, *Phys. Rev. Lett.*, 2000, **84**, 518.
23 T. Landh, *FEBS Lett.*, 1995, **369**, 13.
24 Y. Han, D. L. Zhang, L. L. Chng, J. L. Sun, L. Zhao, X. D. Zou and J. Y. Ying, *Nat. Chem.*, 2009, **1**, 123.
25 S. T. Hyde, L. de Campo and C. Oguey, *Soft Matter*, 2009, **5**, 2782.
26 L. de Campo, M. Moghaddam, T. Varslot, S. T. Hyde, in preparation.
27 R. Strey, J. Winkler and L. Magid, *J. Phys. Chem.*, 1991, **95**, 7502.
28 G. Porod, *Kolloid Z. Z. Polym.*, 1951, **124**, 83.
29 L. de Campo, M. Moghaddam, S. T. Hyde, in preparation.
30 E. M. J. Kampouris, *J. Chem. Soc.*, 1965, 2651.
31 P. Oswald and P. Pieranski, *Smectic and columnar liquid crystals*, CRC Press, 2006.
32 G. Porod, in *Small Angle X-Ray Scattering*, ed. O. Glatter and O. Kratky, Academic Press Inc. (London) Ltd, London, 1982, p. 17.
33 K. Schmidt-Rohr, *J. Appl. Crystallogr.*, 2007, **40**, 16.
34 T. Varslot, *et al.*, in preparation.
35 J. M. Seddon, *Biochim. Biophys. Acta*, 1990, **1031**, 1.
36 W. Pisula, Z. Tomovic, C. Simpson, M. Kastler, T. Pakula and K. Mullen, *Chem. Mater.*, 2005, **17**, 4296.
37 C. Corno, S. Ghelli, G. Perego and E. Platone, *Colloid Polym. Sci.*, 1991, **269**, 1133.
38 P. M. Duesing, R. H. Templer and J. M. Seddon, *Langmuir*, 1997, **13**, 351.
39 J. J. K. Kirkensgaard, S. T. Hyde, in preparation.
40 T. Gemma, A. Hatano and T. Dotera, *Macromolecules*, 2002, **35**, 3225.
41 K. Shinoda and T. Nomura, *J. Phys. Chem.*, 1980, **84**, 365.
42 F. Michaux, J. L. Blin and M. J. Stebe, *J. Phys. Chem. B*, 2008, **112**, 11950.
43 F. Michaux, J. L. Blin and M. J. Stebe, *Langmuir*, 2007, **23**, 2138.